Batteries & Supercaps

Research Article
doi.org/10.1002/batt.202400404

Chemistry Europe
European Chemical Societies Publishing

www.batteries-supercaps.org

VIP *Very Important Paper*

Effects of SiO_2 Particle Size in Soggy-Sand Electrolyte on Electrochemical Performance of Zinc-Ion Batteries

Jieshuangyang Chen,[a] Rongyu Deng,[a] Jinwei Zhou,[a] Ziang Jiang,[a] Mingzhi Qian,[a] and Feixiang Wu*[a]

The presence of free water molecules in the aqueous electrolyte leads to serious side reactions at the interface, easy dissolution of the cathode material, and uncontrolled growth of zinc dendrites in Zn-ion batteries, which hinders their practical applications. Here, we propose a type of SiO_2-based soggy-sand electrolyte ($ZnSO_4 + MnSO_4$ electrolyte with SiO_2, SiO_2-$ZMSO_4$) and focus on the effect of the SiO_2 nanoparticle size on the performance of soggy-sand electrolyte. It is found that SiO_2 with smaller nanoparticle size provides higher porosity, and the SiO_2 network-formed can effectively trap the free water in the electrolyte, which increases the ionic conductivity of electrolyte, widens working voltage window, and decreases the internal resistance of batteries. As a result, the Zn//MnO_2 batteries with 20 nm SiO_2-based soggy-sand electrolyte show stable cycling performance and rate capacities. The specific capacity of the battery can be maintained at 198.5 mAh g^{-1} after 1200 cycles at 1 A g^{-1} without capacity degradation. The specific capacity can be increased by 100 mAh g^{-1} even at a high rate of 5 A g^{-1}. This study provides the rule of particle selection for the development of aqueous soggy-sand electrolytes used in aqueous rechargeable batteries.

Introduction

The development of renewable energy sources with safety is considered as an important direction in the field of large-scale energy storage.[1–3] Compared to aqueous lithium-ion batteries, aqueous zinc-ion batteries (ZIBs) exhibit numerous advantages, including lower cost, greater zinc abundance, enhanced safety, heightened cycle stability, and improved environmental friendliness. Consequently, ZIBs stand as an emerging and environmentally friendly energy storage solution, demonstrating significant potential for widespread applications.[4–7]

However, the widespread commercialization of aqueous ZIBs faces significant obstacles. Particularly, there are serious side reactions in mildly acidic conditions, giving rise to two primary issues: the evolution of hydrogen gas (H_2) and the precipitation of alkaline Zn sulfate ($Zn(OH)_2{\cdot}ZnSO_4{\cdot}nH_2O$). These side reactions, occurring during the continuous charge and discharge cycles of ZIBs, result in uncontrolled zinc dendrites growth. The persistent challenges of dendrite growth and unwanted side reactions on the Zn anode seriously compromise the interface between Zn anode and electrolyte, leading to an overall decline in battery performance. To address these challenges, it is crucial to reduce the reactivity of water molecules and minimize direct contact between the Zn anode and electrolyte, as these strategies are key to enabling the practical application of ZIBs.[8–12]

To date, significant progresses were made in addressing these challenges.[9] Several promising approaches have been explored, e.g.: increasing the salt concentration to enhance the interaction between the water and salt anions/cations,[13] adding organic electrolytes to improve interfacial stability of Zn anode,[14] decoupling the Zn^{2+} solvation shell or forming hydrogen bonds with water with the help of ligands can suppress water activity,[15,16] and constructing advanced interfaces to avoid direct contact between the water and Zn anode.[17] All these methods are aimed at reducing battery side reactions by inhibiting the high activity of water molecules or constructing special interfaces to reduce the possibility of direct contact between water and the anode. Among these approaches, gel/colloidal electrolytes have also been studied and developed for their safety, biocompatibility, and abundance.[18]

Sun et al. had investigated the effect of particle sheer size on the gelation of fumed SiO_2 in sulfuric acid medium of valve-regulated lead-acid batteries.[19] The results show that the strength of the gel increased with the increase of particle size. However, at the same SiO_2 content, the increase in particle size leads to a decrease in particle density, which greatly weakens the three-dimensional structure of the SiO_2 particle network and reduces the efficiency of ion transfer. In a subsequent research, Liu et al. prepared a flexible gel electrolyte for zinc//manganese dioxide (Zn//MnO_2) battery by adding SiO_2 nanoparticles into the polymer electrolyte.[20] The gel electrolyte with SiO_2 nanoparticles possesses a high ionic conductivity, and the fire retardancy of the ionogel electrolyte is also improved. It is expected to realize the high requirements of wearable electronic devices for flexible batteries. The studies utilized SiO_2, an inert inorganic material, as an electrolyte additive, which can combine with water in the electrolyte and effectively reduces the activity of water.[20–22]

[a] J. Chen, R. Deng, J. Zhou, Z. Jiang, M. Qian, F. Wu
School of Metallurgy and Environment, National Engineering Research centre of Advanced Energy Storage Materials, Central South University, Changsha 410083, China
E-mail: feixiang.wu@csu.edu.cn

Supporting information for this article is available on the WWW under https://doi.org/10.1002/batt.202400404

Research Article
doi.org/10.1002/batt.202400404
Chemistry Europe
European Chemical Societies Publishing

Recently, aqueous soggy-sand electrolytes were developed for high-performance ZIBs. The selection of SiO_2 particles for constructing suitable soggy-sand electrolytes is very important. Here, following the previous studies on soggy-sand electrolyte,[23] effects of SiO_2 particle size in soggy-sand electrolyte on electrochemical performance of ZIBs were studied. By adding a small amount of SiO_2 to $ZnSO_4+MnSO_4$ solution (SiO_2-$ZMSO_4$, soggy-sand electrolyte), an electrolyte with a morphology like gel electrolyte but with certain fluidity was prepared, and used in Zn//MnO_2 batteries. The smaller particle size of SiO_2, the denser pore structure on the surface, which can combine well with free water molecules, thus greatly reducing the content of free water molecules in the electrolyte, and further reducing the internal side reactions of the battery. As a result, compared with the pure $ZnSO_4+MnSO_4$ electrolyte ($ZMSO_4$, conventional electrolyte) and 1 μm-SiO_2-$ZMSO_4$ electrolyte, the introduction of the 20 nm SiO_2 resulted in a superior specific capacity, higher Coulombic efficiency and longer cycle life. A specific capacity of 198.49 mAh g^{-1} can be maintained after 1200 cycles at 1 A g^{-1} without capacity degradation. It is worth noting that changing only one variable, the SiO_2 particle size, can bring about a 111.5 mAh g^{-1} specific capacity improvement. At a higher rate of 5 A g^{-1}, there is still an increase in specific capacity of 100 mAh g^{-1}.

Results and Discussion

The XRD images in Figure 1a show that both 20 nm SiO_2 samples and 1 μm SiO_2 samples are single phase. From the SEM/EDS (Scanning Electron Microscope/Energy Dispersive Spectrometer) images (Figure 1b), it can be observed that the particle sizes of the 20 nm SiO_2 and the 1 μm SiO_2 are uniform, and the both samples only contain Si and O elements without other substances. From the morphological point of view, the particles of 20 nm SiO_2 are in regular spherical shape, while the particles of 1 μm SiO_2 are in irregular morphology. The adsorption and desorption isotherms of 20 nm SiO_2 and 1 μm SiO_2 are shown in Figure 1c and d, respectively. Here, the adsorption-desorption behaviors of the two SiO_2 materials with different particle sizes are reversible without any obvious hysteresis. SiO_2 has an internal microporous structure.[24] Compared to 1 μm SiO_2, 20 nm SiO_2 provides a larger specific surface area (150.52 $m^2 g^{-1}$) and higher porosity (pore volume of 0.304 $cm^3 g^{-1}$). Due to the capillary force at the pore seams or at the pore mouth, more water molecules can be pumped into the 20 nm SiO_2 porous space for binding, which can effectively inhibit the occurrence of side reactions.[25]

Complete soggy-sanding of the electrolyte would result in weaker fluidity and lower conductivity. Considering this, it chose to blend a 5 wt.% (Figure S1, Supporting Information, SiO_2 amount optimization) electrolyte solution (5 wt.% SiO_2 + 95 wt.% $ZMSO_4$) to form a kind of soggy-sand electrolyte, which still has good mobility and high conductivity while soggy-sanding. Four SiO_2 powders with different particle sizes (20 nm,

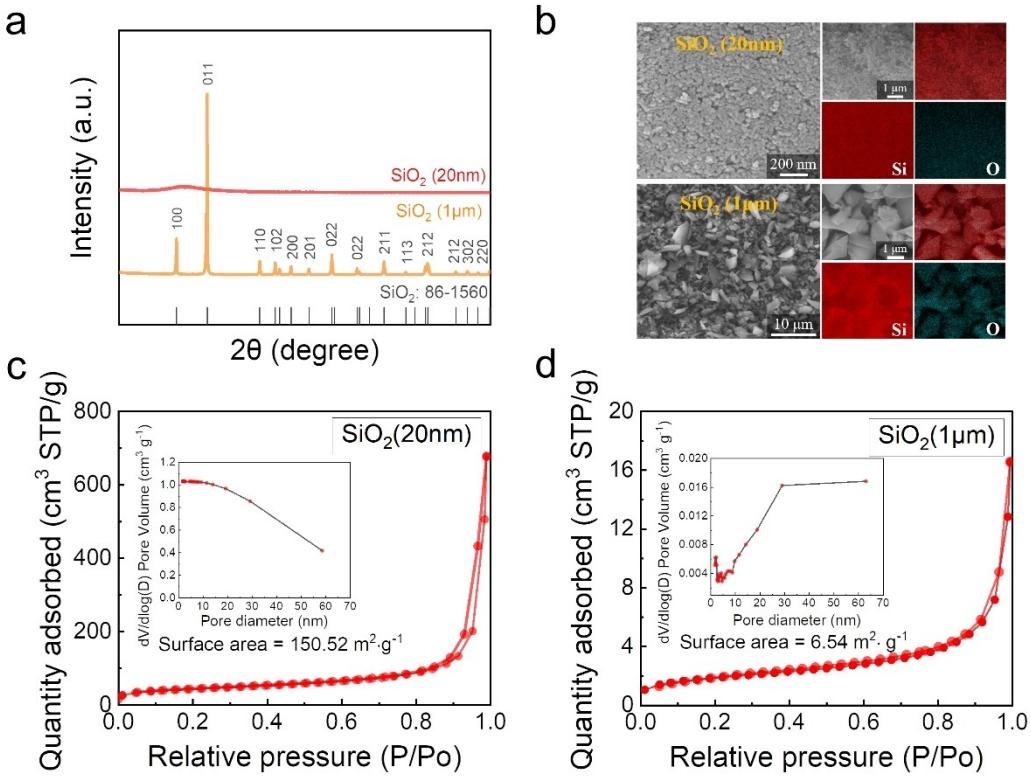

Figure 1. Basic characterization of SiO_2 samples (electrolyte additives): **a**. XRD patterns of SiO_2 sample after drying; **b**. SEM/EDS images of SiO_2 samples; **c, d**. Nitrogen adsorption and desorption isotherms of the SiO_2 materials.

Research Article
doi.org/10.1002/batt.202400404
Chemistry Europe
European Chemical Societies Publishing

500 nm, 1 μm, 10 μm) were selected and 1.0 g SiO_2 powder was added to 19 g $ZMSO_4$ electrolyte, respectively, and mixed to obtain the SiO_2-based soggy-sand electrolytes, whose optical photographs are shown in Figure 2a. Combined with Figure 2b, it is found that nanoscale SiO_2 (nanoscale particle sizes, 20 nm and 500 nm) combined with the electrolyte is more likely to form a soggy-sand state with low viscosity and good flowability. After two hours of standing (Figure 2c), the soggy-sand electrolyte with nanoscale SiO_2 is homogeneously mixed, while the separation and precipitation of SiO_2 and $ZMSO_4$ electrolyte in the soggy-sand electrolyte with microscale SiO_2 (microscale particle sizes, 1 μm and 10 μm) occurs, which indicates that the nanoscale SiO_2 has a stronger binding energy with the water molecules in the electrolyte. In order to further investigate the stability of the electrolyte after the addition of SiO_2, measured the Differential Scanning Calorimetry (DSC) curves of the five electrolytes in the range of −60–20 °C, as shown in Figure 2d. The DSC curves of all five electrolytes show similar heat absorption steps around −12 °C, indicating that neither the presence of SiO_2 nor the particle size of SiO_2 have much effect on the melting process of the electrolyte. At −44.1 °C, an exothermic step appears in the DSC curve of the $ZMSO_4$ electrolyte, and this exothermic process corresponds to the glass transition. The glass transition temperatures of the electrolytes were all reduced by about 10 °C after the addition of SiO_2. The glass transition temperature gradually decreases with the increase of SiO_2 particle size, which indicates that the viscosity of soggy-sand electrolyte with nanoscale SiO_2 is greater than that of soggy-sand electrolyte with microscale SiO_2, and also proved that the binding energy between nanoscale SiO_2 and $ZMSO_4$ electrolyte is higher from the side.[26] High ionic conductivity is a unique advantage of aqueous electrolytes, and it need to conduct further tests considering the effect of SiO_2 materials on ionic conductivity. As shown in Figure 2e, comparing the conductivity of the conventional $ZMSO_4$ electrolyte without SiO_2 addition (51.3 mS cm^{-1}), the conductivity of the soggy-sand electrolyte with nanoscale SiO_2 is unchanged or higher (20 nm, 52 mS cm^{-1}; 500 nm, 51.3 mS cm^{-1}), but the conductivity of the soggy-sand electrolyte with microscale SiO_2 (1 μm, 49.8 mS cm^{-1}; 10 μm, 47.8 mS cm^{-1}) are lower than those of $ZMSO_4$ electrolyte. In the aqueous $ZMSO_4$ electrolyte, most of the $ZnSO_4$ dissociates into Zn^+ and SO_4^{2-} ions under the force of H_2O molecules, but a small amount of $ZnSO_4$ still exists in molecular form.

Regardless of the particle sizes of SiO_2 added, it dissociates a small amount of $ZnSO_4$ molecules, thus increasing the conductivity of the electrolyte. After standing for a longer time (10 days in a thermostat at 25 °C), the SiO_2 in the soggy-sand electrolyte undergoes partial precipitation, resulting in a decrease in conductivity. As a result, the conductivity of all the soggy-sand electrolyte tends to increase and then decrease, and the conductivity of the aqueous $ZMSO_4$ electrolyte remains essentially constant.

Based on the above characteristics, the mixed electrolyte after adding SiO_2 is suitable for aqueous Zn/MnO_2 batteries, which can effectively reduce the activity of water in the electrolyte and inhibit the occurrence of side reactions. Here, we selected 20 nm-SiO_2-$ZMSO_4$ electrolyte and 1 μm-SiO_2-$ZMSO_4$ electrolyte to assemble the batteries with Zn anode and MnO_2 cathode for electrochemical tests. Figure 3a shows the Linear Sweep Voltammetry (LSV) curves of the three electrolytes. The decomposition voltages of $ZMSO_4$ electrolyte and 1 μm-SiO_2-$ZMSO_4$ electrolyte are basically the same at the same current, and the 20 nm-SiO_2-$ZMSO_4$ electrolyte has a larger decomposition voltage showing a wider stabilized voltage window compared with these two electrolytes. The Open

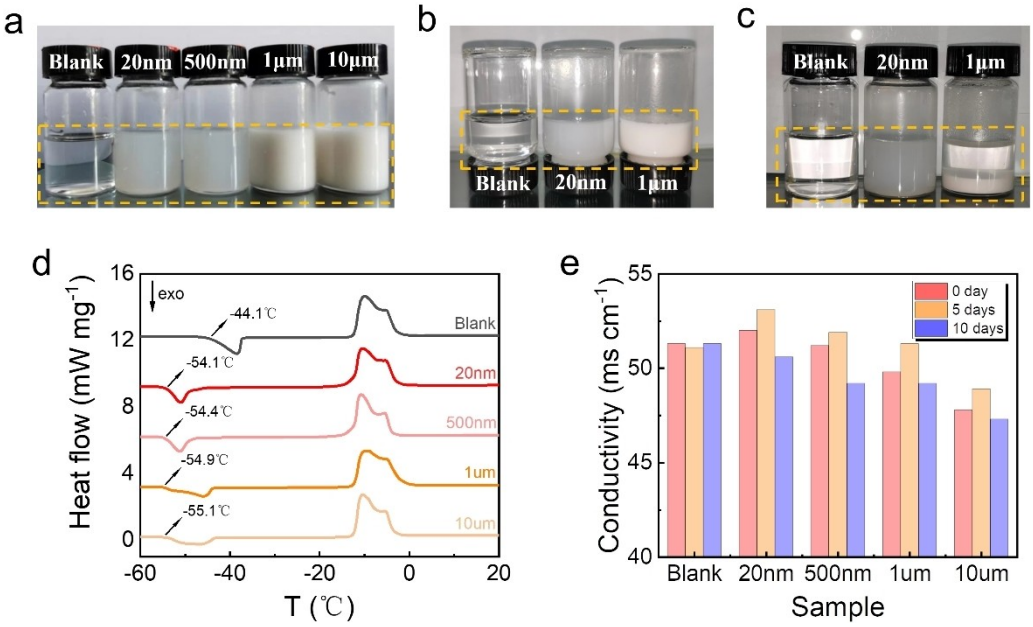

Figure 2. Characterization of various electrolytes: **a, b, c**. Optical photomicrographs of various electrolytes; **d**. Differential heat flow versus temperature curves (DSC curves) for different electrolytes; **e**. Electrical conductivity of different electrolytes.

Research Article
doi.org/10.1002/batt.202400404
Chemistry Europe
European Chemical Societies Publishing

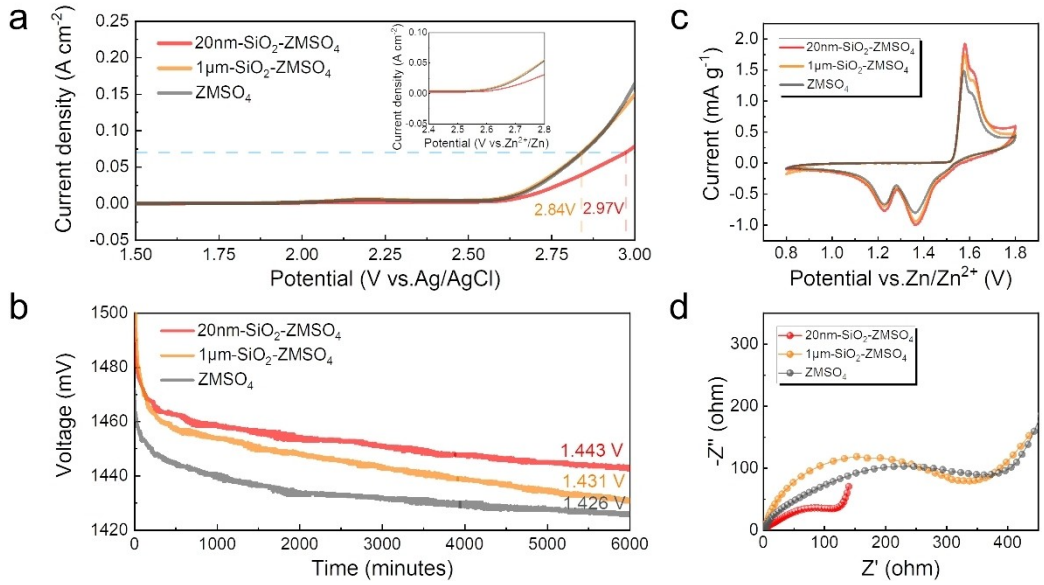

Figure 3. Electrochemical characterization test: **a**. LSV curves of the batteries with 20 nm-SiO_2-$ZMSO_4$, 1 μm-SiO_2-$ZMSO_4$ and $ZMSO_4$ electrolyte; **b**. Monitoring the open-circuit voltages of the three batteries after 6000 minutes; **c**. Comparison of CV scanning of batteries with different electrolytes from 0.8 to 1.8 V (1 mV s^{-1}, second cycle); **d**. The EIS of batteries with various electrolytes before cycling.

Circuit Voltage (OCV) of a battery directly responds to the state of electrochemical reactions in the battery, and can also provide information such as battery internal resistance test and energy loss, which has gained extensive attention from previous studies.[22,27] The batteries in the electrolytes of 20 nm-SiO_2-$ZMSO_4$, 1 μm-SiO_2-$ZMSO_4$, and $ZMSO_4$ electrolytes were left to stand for 6000 minutes after complete activation and the open-circuit voltages (OCVs) of the batteries are shown in Figure 3b. The OCV of the battery is enhanced by the addition of SiO_2 compared with that of the battery with $ZMSO_4$ electrolyte, and the OCV of the battery with SiO_2-$ZMSO_4$ electrolyte is still higher than that of the battery with $ZMSO_4$ electrolyte after 6000 minutes of resting. When the potential difference of the battery is certain, the internal resistance of the battery affects the OCV test results, and SiO_2 can reduce the activity of water and thus inhibiting the occurrence of side reactions, so that the internal resistance of the battery decreases and the OCV becomes larger. Comparing the batteries with different particle sizes of SiO_2 added, the OCV decrease of the battery with 20 nm-SiO_2-$ZMSO_4$ electrolyte is significantly lower than that of the battery with 1 μm-SiO_2-$ZMSO_4$ electrolyte, which indicates that 20 nm SiO_2 has a stronger inhibiting effect on the activity of water in the electrolyte. Figure 3c shows the cyclic voltammetry (CV) curves of Zn/MnO_2 batteries in different electrolytes. The addition and absence of SiO_2 show similar redox behavior, indicating that the presence of SiO_2 does not affect the redox reaction of the MnO_2 cathode. However, the batteries with SiO_2-added electrolytes show lower internal resistance compared to those with conventional electrolytes, especially those assembled with electrolytes incorporating 20 nm SiO_2, which show significantly lower charge transfer impedance and display faster reaction kinetics and superior electrochemical interfaces (Figure 3d).

To further investigate the effect of SiO_2 particle size on the electrochemical performance, Zn/MnO_2 batteries were assembled with the $ZMSO_4$ conventional electrolyte and SiO_2-$ZMSO_4$ soggy-sand electrolyte, which incorporates SiO_2 with different particle sizes. As shown in Figure 4a, the battery with $ZMSO_4$ conventional electrolyte exhibits a significant decay at a current density of 1 A g^{-1}, with a capacity retention of 47% after 500 cycles. In contrast, the batteries with the SiO_2-based soggy-sand electrolyte exhibit higher specific capacity and more stable cycling performance, and the smaller particle size of SiO_2 is more favorable for capacity retention. The initial specific capacity of the battery with 20 nm-SiO_2-$ZMSO_4$ electrolyte is 178 mAh g^{-1} at 1 A g^{-1} current density, and maintained at 183 mAh g^{-1} with a coulombic efficiency close to 100% without capacity decay after 500 cycles. Their corresponding charge and discharge curves after different cycles indicate that the voltage polarization in the soggy-sand electrolyte is reduced compared with that in the conventional electrolyte, especially in the 20 nm-SiO_2-$ZMSO_4$ electrolyte, the polarization reduction is more obvious, and it exhibits a better redox platform and faster reaction kinetics (Figure 4b). The long-term cycling performance of the batteries with $ZMSO_4$ electrolyte and 20 nm-SiO_2-$ZMSO_4$ electrolyte are further evaluated at 1 A g^{-1} (Figure 4c). In contrast, the battery with $ZMSO_4$ electrolyte shows significant degradation from 80 mAh g^{-1} to 45 mAh g^{-1} after 500 cycles. It is worth noting that the initial specific capacity of the battery with 20 nm-SiO_2-$ZMSO_4$ electrolyte is 157 mAh g^{-1}, and maintained at 199 mAh g^{-1} without capacity degradation and a coulombic efficiency of nearly 100% after 1200 cycles. The charge and discharge curves of the batteries with 20 nm-SiO_2-$ZMSO_4$ electrolyte maintain a good and stable voltage plateau at different cycle times, showing a long cycle life and stable cycling performance (Figure 4d). The reaction rates of batteries

Research Article
doi.org/10.1002/batt.202400404
Chemistry Europe
European Chemical Societies Publishing

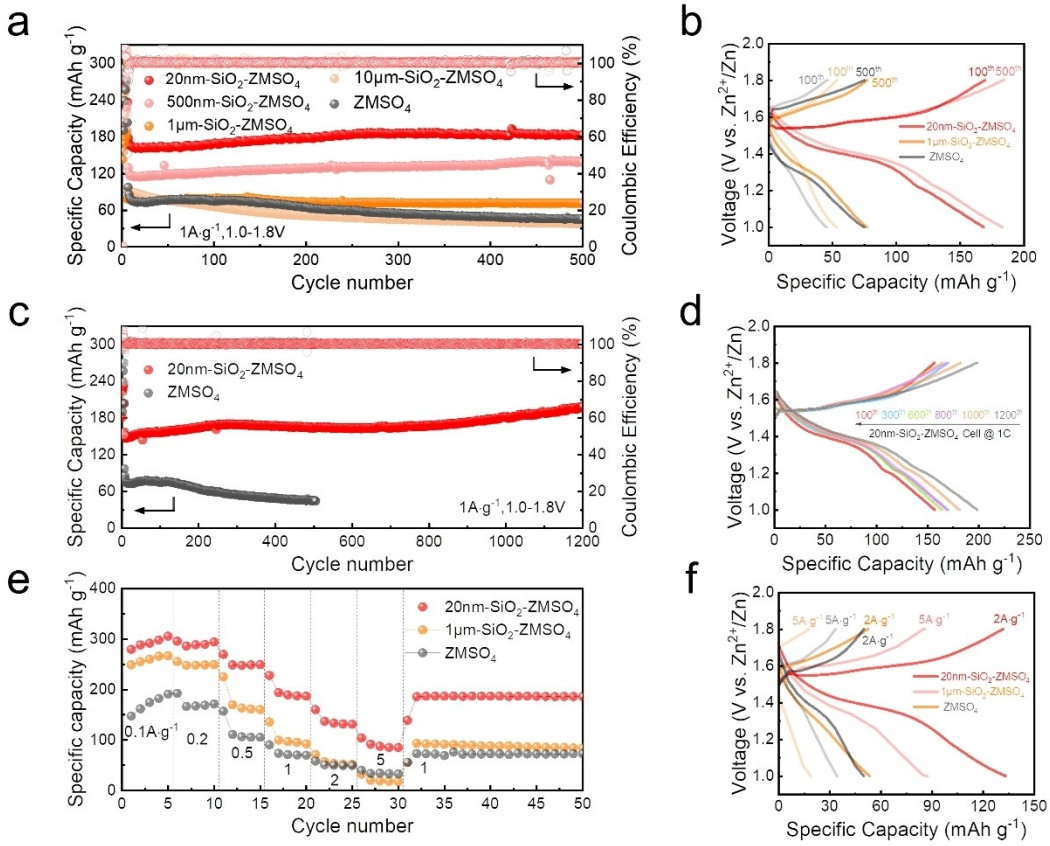

Figure 4. Electrochemical performance of Zn/MnO_2 batteries: **a**. Long-term cycling performance in various electrolytes at a current density of 1 A g^{-1}; **b**. Charge and discharge curves at 100th and 500th cycles for various batteries; **c**. Long-term cycling performance in 20 nm-SiO_2-$ZMSO_4$ electrolyte at a current density of 1 A g^{-1}; **d**. Charge and discharge curves to different cycles; **e**. The rate performance of batteries in various electrolytes; **f**. Charge and discharge curves at different multiplicities.

with different electrolytes at various current densities are shown in Figure 4e. Compared with the batteries with $ZMSO_4$ electrolyte, the average discharge specific capacities of the battery with 20 nm-SiO_2-$ZMSO_4$ electrolyte were 300, 290, 248, 189, 133, and 87 mAh g^{-1} at the current density range from 0.1 to 5 A g^{-1}, respectively, and the high specific capacities and fast reaction kinetics are still observed even at the high current density of 5 A g^{-1}. More importantly, when the current density applied to the battery is restored to 1 A g^{-1}, the specific capacity of the battery with 20 nm-SiO_2-$ZMSO_4$ electrolyte is recovered to 187 mAh g^{-1}. In contrast, the battery with 1 μm-SiO_2-$ZMSO_4$ electrolyte has a lower specific discharge capacity at current densities ranging from 0.1 to 5 A g^{-1}. In the current densities of 2 A g^{-1} and 5 A g^{-1}, the discharge specific capacity of the battery only reaches 53 mAh g^{-1} and 19 mAh g^{-1}, and recovers to 87 mAh g^{-1} at 1 A g^{-1} current density, which is almost the same as the battery with conventional electrolyte. It can be observed that the specific capacity of the battery is higher as the particle size of SiO_2 added to the electrolyte decreases. Especially, at high current densities, the kinetics of the battery with 20 nm-SiO_2-$ZMSO_4$ electrolyte is significantly better than the battery with 1 μm-SiO_2-$ZMSO_4$ electrolyte. In addition, the corresponding charge and discharge curves exhibit less voltage polarization in the electrolyte with 20 nm SiO_2 incorporated (Figure 4f).

MnO_2 cathodes and Zn anodes were obtained after 1000 cycles at 1 A g^{-1} to study the electrochemical deposition behavior of different batteries during repeated cycles. The SEM images show that more MnO_2 is deposited on the cathode of the battery with 20 nm-SiO_2-$ZMSO_4$ electrolyte and the overall morphology is well preserved (Figure 5a and b). However, the significantly less MnO_2 on the cathode with 1 μm-SiO_2-$ZMSO_4$ electrolyte and shows obvious dissolution features (Figure 5c and d). Similarly, post mortem examination was performed of the battery after 1000 cycles to analyze the Zn anode surface. The SEM images of the anode with 20 nm-SiO_2-$ZMSO_4$ electrolyte show a very smooth and flat surface (Figure 5e and f), and there are no dendrites on the Zn anode surface. In contrast, the dendrite shape can be clearly seen in the SEM images of the anode with 1 μm-SiO_2-$ZMSO_4$ electrolyte after cycling, and there is obvious dendrite growth on the anode surface after operation, which accumulates a lot of by-products (Figure S2, Supporting Information). The by-products in contact with the electrolyte can cause serious corrosion and hydrogen precipitation problems, which is not favorable for the large-scale practical application of aqueous ZIBs.[28] The results show that SiO_2 particle size can significantly affect the existence form of

Research Article
doi.org/10.1002/batt.202400404
Chemistry Europe
European Chemical Societies Publishing

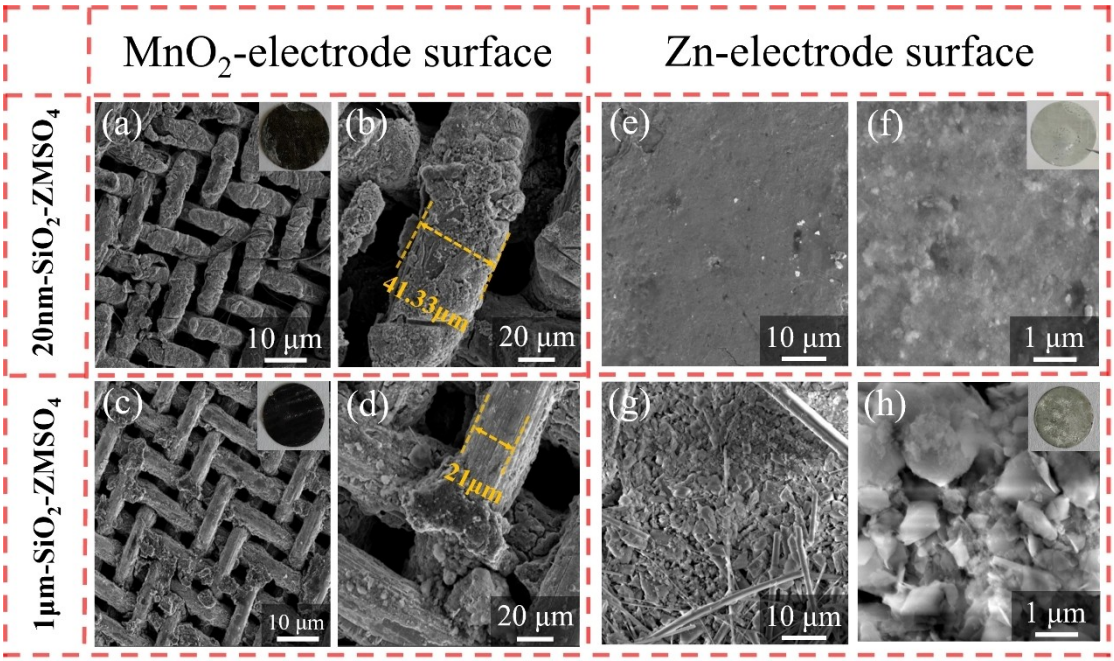

Figure 5. Electrode morphology after cycling: **a, b, c, d**. SEM images of MnO_2 cathode after 1000 cycles in 20 nm-SiO_2-$ZMSO_4$ electrolyte and 1 μm-SiO_2-$ZMSO_4$ electrolyte; **e, f, g, h**. SEM images of Zn anode after 1000 cycles in 20 nm-SiO_2-$ZMSO_4$ electrolyte and 1 μm-SiO_2-$ZMSO_4$ electrolyte. (Photographs of the electrode surface after 1000 cycles, illustrations).

cathode substance Mn and the deposition morphology on the Zn anode surface. The smaller SiO_2 particle size, the more effective it is to inhibit the MnO_2 dissolution and regulate the Zn deposition, improving the overall reaction kinetics and maintaining the structural stability of electrode.

Conclusions

In summary, this study proposes a novel and practical electrolyte by adding SiO_2 with different particle sizes to the conventional electrolyte and revealing its effectiveness in ZIBs. SiO_2 with smaller particle size has greater surface porosity and stronger interaction force with free water in the electrolyte, significantly improving the overall reactivity inside the battery. Compared with the1 μm-SiO_2-$ZMSO_4$ electrolyte, the 20 nm-SiO_2-$ZMSO_4$ electrolyte suppressed the side reactions, inhibited the dissolution of the cathode and reduced the interfacial corrosion and passivation of the anode. Meanwhile, the discharge specific capacity of battery was improved and the electrochemical stability window was expanded. These results show that changing only one small variable, the SiO_2 particle size, enables the battery to exhibit better performance in terms of multiplier capacity and cycle stability. The Zn//MnO_2 battery with 20 nm-SiO_2-$ZMSO_4$ electrolyte has long-term cycling stability in the voltage range of 1.0–1.8 V with a current density of 1 $A\,g^{-1}$. The average discharge specific capacity of the battery exceeds 160 $mAh\,g^{-1}$ after 1200 cycles, and realizes extraordinary rate capability at 0.1–5 $A\,g^{-1}$. This work demonstrates that SiO_2 with smaller particle size can greatly affect the electrolyte capability, which further affects the electrochemical performance of ZIBs. This provides a new research idea for subsequent electrolyte optimization schemes for aqueous rechargeable batteries.

Experimental Section

Preparation of electrolytes. A solution of 2 M $ZnSO_4$ + 0.1 M $MnSO_4$ was prepared as a conventional electrolyte by adding 57.4 g of $ZnSO_4{\cdot}7H_2O$ (Aladdin, AR) and 1.6902 g of $MnSO_4{\cdot}H_2O$ (Aladdin, 99%) in DI water, which was adjusted to 100 mL to form a solution of 2 M $ZnSO_4$ + 0.1 M $MnSO_4$, where a small amount of $MnSO_4$ was added in order to inhibit the dissolution of Mn in the cathode material. SiO_2 with different particle sizes (20 nm, 500 nm, 1 μm, 10 μm) was added to the conventional electrolyte to prepare 5 wt% soggy-sand electrolytes for experiments. It was shaken and stirred until well dispersed.

Anode materials synthesis. The anode material was MnO_2, synthesized according to the method reported in the relevant literature.[29] First, 0.1 g of carbon nanotubes (CNTs) was added to 60 mL of DI water and dispersed by ultrasonication for 15 min, then 0.486 g of $KMnO_4$ was added to the solution and stirred for 30 min until the solution was completely mixed well. Later, 1.135 g of Mn $(CH_3COO)_2{\cdot}4H_2O$ was added to 20 mL of deionized water and stirred for 15 min until the salt was completely dissolved. After that, the two prepared solutions were slowly mixed and dispersed by ultrasonication for 60 min at room temperature. Finally, the well-mixed solution was transferred to an autoclave reactor and heated at 120 °C for 12 h. After the completion of hydrothermal, the final product, manganese dioxide, was obtained after washing, filtration, and freeze-drying.

Material Characterization. The experimental samples SiO_2 were examined using an X-ray diffractometer (XRD, PANalytical) equipped with an 8 Kev Cu Ka radiation source, with a scan rate of

5°/min and a scan range of 5°–80°. Scanning electron microscopy (SEM, Tescan/Clara) was used to image the material SiO_2, cathode, and anode after battery operation. Thermogravimetric analysis of SiO_2 was performed using a thermogravimetric-infrared-gas chromatography-mass spectrometry analyzer (Platinum Elmer/TGA/STA8000-FTIR-GCMS-ATD). SiO_2 was characterized on a fully automated specific surface and porosity analyzer (BET, Micromeritics ASAP 2460) using a nitrogen adsorption-desorption procedure.

Electrochemical measurements. The prepared cathode materials MnO_2, polyvinylidene fluoride (PVDF), and super P were mixed and formulated in the mass ratio of 7:2:1, and a certain amount of NMP was added as a solvent, then stirred at 25 °C for 12 h. The modulated slurry was uniformly coated on the stainless-steel wire mesh (SSWM), and dried in a vacuum oven at 80 °C for 24 h. The electrode sheets were prepared into a diameter of 10 mm by using the sheet punching machine, small discs as cathode electrodes. Here, the amount of cathode active substance was determined by the mass of MnO_2 coated on the stainless-steel wire mesh, and the load of active substance used for the experiments was controlled at 0.8–1.0 mg cm^{-2}, the theoretical specific capacity of the battery was calculated based on the mass of active substance MnO_2. The polished and sanded Zn metal foil was prepared into small discs with a thickness of 0.1 mm and a diameter of 12 mm as anode electrodes using a sheet punching machine. A Zn//MnO_2 battery was assembled in a CR2032 coin battery using a glass fiber spacer (GF/D) with a diameter of 19 mm as a separator, taking 350 μL of electrolyte, MnO_2 as a cathode and Zn foil as anode. Charge and discharge performance study experiments were carried out for all batteries on a multichannel test system (LAND, China) at a constant temperature of 25 °C. The set voltage range was 1.0–1.8 V, and the current densities ranged from 0.1 to 5 A g^{-1}. Cyclic voltammetry (CV) tests were carried out on a Gamry electrochemical workstation, and the scanning rate was set to 0.1 mV s^{-1}. Electrochemical impedance spectroscopy (EIS) tests were also performed, with picking point frequencies selected from 0.01 to 100 KHz. All electrochemical data were obtained at approximately 25 °C.

Acknowledgements

The authors gratefully acknowledge the National Natural Science Foundation of China (No. 51904344 and No. 52172264) and the Natural Science Foundation of Hunan Province of China (Grant No. 2021JJ10060 and No. 2022GK2033).

Conflict of Interests

The authors declare no conflicts of interest.

Data Availability Statement

The data that support the findings of this study are available from the corresponding author upon reasonable request.

Keywords: Aqueous electrolyte · Nanoparticle additives · Silicon dioxide · Soggy-sand · Zinc-ion battery

[1] S. Guo, L. P. Qin, T. S. Zhang, M. Zhou, J. Zhou, G. Z. Fang, S. Q. Liang, *Energy Stor. Mater.* **2021**, *34*, 45–562.
[2] Y. Yu, J. Maier, F. Wu, *Chem. Soc. Rev.* **2020**, *49*, 1569.
[3] L. S. Wu, Y. F. Dong, *Energy Stor. Mater.* **2021**, *41*, 715–737.
[4] J. M. Tarascon, M. Armand, *Nature* **2001**, *414*, 359–367.
[5] F. Wang, O. Borodin, T. Gao, X. Fan, W. Sun, F. Han, A. Faraone, J. A. Dura, K. Xu, C. Wang, *Nat. Mater.* **2018**, *17*, 543–549.
[6] G. L. Li, Z. Yang, Y. Jiang, W. X. Zhang, Y. H. Huang, *J. Power Sources* **2016**, *308*, 52–57.
[7] J. N. Hao, X. L. Li, X. H. Zeng, D. Li, J. F. Mao, Z. P. Guo, *Energy Environ. Sci.* **2020**, *13*, 3917–3949.
[8] X. Zeng, K. Xie, S. Liu, S. Zhang, J. Hao, J. Liu, W. K. Pang, J. Liu, P. Rao, Q. Wang, J. Mao, Z. Guo, *Energy Environ. Sci.* **2021**, *14*, 5947–5957.
[9] B. Y. Tang, L. T. Shan, S. Q. Liang, J. Zhou, *Energy Environ. Sci.* **2019**, *12*, 3288–3304.
[10] W. C. Du, E. H. X. Ang, Y. Yang, Y. F. Zhang, M. H. Ye, C. C. Li, *Energy Environ. Sci.* **2020**, *13*, 3330–3360.
[11] Z. Y. Xing, G. F. Xu, X. S. Xie, M. J. Chen, B. G. Lu, J. Zhou, S. Q. Liang, *Nano Energy* **2021**, *90*, 106621.
[12] D. Lin, Y. Li, *Adv. Mater.* **2022**, *34*, 2108856.
[13] L. Suo, Y. S. Hu, H. Li, M. Armand, L. Chen, *Nat. Commun.* **2013**, *4*, 1481.
[14] S. D. Han, N. N. Rajput, X. Qu, B. Pan, M. He, M. S. Ferrandon, C. Liao, K. A. Persson, A. K. Burrell, *ACS Appl. Mater.* **2016**, *8*, 3021–3031.
[15] Q. Zhang, Y. Ma, Y. Lu, X. Zhou, L. Lin, L. Li, Z. Yan, Q. Zhao, K. Zhang, J. Chen, *Angew. Chem. Int. Ed.* **2021**, *133*, 23545–23552.
[16] N. Wang, Y. Yang, X. Qiu, X. Dong, Y. Wang, Y. Xia, *ChemSusChem* **2020**, *13*, 5556–5564.
[17] J. H. Park, M. J. Kwak, C. Hwang, K. N. Kang, N. Liu, J. H. Jang, B. A. Grzybowski, *Adv. Mater.* **2021**, *33*, 2101726.
[18] W. H. Yang, Y. Yang, H. J. Yang, H. S. Zhou, *ACS Energy Lett.* **2022**, *7*, 2515–2530.
[19] X. X. Sun, J. X. Zhao, T. X. Chen, X. W. Liu, *J. Solid State Electrochem.* **2015**, *20*, 657–664.
[20] J. Liu, N. Y. Nie, H. Wang, Z. Chen, Z. Y. Ji, X. F. Duan, Y. Huang, *Soft Matter.* **2020**, *16*, 7432–7437.
[21] Y. Q. Liao, L. X. Yuan, X. T. Liu, J. T. Meng, W. Zhang, Z. Li, Y. H. Huang, *Energy Stor. Mater.* **2022**, *48*, 366–374.
[22] C. Y. Lu, T. K. A. Hoang, T. N. L. Doan, H. B. Zhao, R. Pan, L. Yang, W. S. Guan, P. Chen, *Appl. Energy.* **2016**, *170*, 58–64.
[23] R. Y. Deng, J. S. Y. Chen, F. L. Chu, M. Z. Qian, Z. J. He, A. W. Robertson, J. Maier, F. X. Wu, *Adv. Mater.* **2024**, *36*, 231153.
[24] J. A. Bau, K. Takanabe, *ACS Catal.* **2017**, *7*, 7931–7940.
[25] C. Y. Lu, T. K. A. Hoang, T. N. L. Doan, M. Acton, H. Zhao, W. Guan, P. Chen, *J. Ind. Eng. Chem.* **2016**, *42*, 101–106.
[26] H. Y. Xu, J. Liu, R. L. Wu, X. Z. Yang, *Mater. Sci.* **2020**, *10*, 980–992.
[27] M. G. Zhang, T. T. Hu, X. Wang, P. Chang, L. Pan, Z. Jin, H. Mei, L. Cheng, L. Zhang, *Energy Stor. Mater.* **2022**, *51*, 465–475.
[28] M. Zhou, Y. Chen, G. Z. Fang, S. Q. Liang, *Energy Stor. Mater.* **2022**, *45*, 618–646.
[29] R. Y. Deng, Z. J. He, F. L. Chu, J. Lei, Y. Cheng, Y. Zhou, F. X. Wu, *Nat. Commun.* **2023**, *14*, 4981.

Manuscript received: June 20, 2024
Revised manuscript received: July 21, 2024
Accepted manuscript online: August 7, 2024
Version of record online: October 4, 2024